DEVELOPMENT OF RESIDUAL STRESS MODEL FOR WELDED BOX SECTIONS USING PROBABILISTIC APPROACH

A. HORVÁTH *, D. KOLLÁR*

**Budapest University of Technology and Economics, Faculty of Civil Engineering, Department of Structural Engineering, H-1111, Budapest, Hungary, horvath.andras@edu.bme.hu*

DOI 10.3217/978-3-99161-089-2-022, license CC BY 4.0

ABSTRACT

Manufacturing processes significantly contribute to the formation of imperfections such as residual stresses and distortions in components. This study focuses on residual stresses induced by welding in box sections made from a combination of normal strength steel (NSS) and high strength steel (HSS) plates. Advanced manufacturing simulations are carried out using a deterministic, uncoupled transient thermomechanical analysis incorporating a double-ellipsoidal heat source model. These simulations evaluate the residual stress distribution in weldments across various steel grades, geometries, and welding parameters (e.g., heat input, welding speed). Furthermore, the study presents a methodology for probabilistic welding simulation. Longitudinal residual stresses are analysed using Monte Carlo simulations with Latin hypercube sampling. The findings support the development of a comprehensive residual stress model that integrates key welding and fabrication characteristics, reflecting the specificities of manufacturing technologies.

Keywords: Welding simulation, Residual stress model, Probabilistic, Box section

INTRODUCTION

All manufacturing processes, welding in particular, inherently introduce residual stresses and distortions, which significantly affect the structural performance, load-bearing capacity, and durability of the products. As welding became the predominant joining method in the last decades in steel construction industry, understanding its effects is essential. Numerical simulations have become a key tool for understanding the behaviour of structures during fabrication, providing insight into geometric imperfections and residual stresses as well. Since distinct residual stress and distortion magnitudes are generated in different base materials in line with the applied welding process, advanced modelling techniques are required to realistically capture these effects. To fully exploit the potentials in simulations,

validated numerical modelling frameworks are required, supported by limited number of physical experiments. This paper presents an experimental and numerical study on welded box sections made from normal strength steel (NSS) and high strength steel (HSS). A finite element-based, stochastic virtual manufacturing approach is proposed to derive residual stress models that reflect actual fabrication conditions. Probabilistic analysis is particularly important, as it enables a systematic investigation of the sensitivity of the residual stress model to its key parameters. Thereby residual stress model parameters are refined, supporting more reliable and sustainable structural design using advanced numerical tools such as geometrically and materially nonlinear analysis including imperfections.

MEASUREMENTS

The validation of the numerical simulations discussed in this conference paper is based on previously conducted experimental investigations. The earlier study [1] concentrated on evaluating residual stresses in box sections made from normal strength steel (NSS - S355MC), high strength steel (HSS - S700MC), and their hybrid (NSS + HSS) configurations. A total of nine specimens featuring single-bevel butt welds were tested (see Fig. 1). The wall thicknesses (t) ranged from 4 mm to 8 mm, the widths (B) of the rectangular cross-sections varied between 200 mm and 220 mm, and the lengths (L) were between 700 mm and 800 mm. The geometric parameters and steel grades of the sections are summarised in Table 1, while the mechanical properties of base materials are presented in Table 2. The welding variables for all the analyzed sections presented in this paper are summarized in Table 3.

Table 1 Measured dimensions and steel grades of all the nine investigated specimens. [1]

Specimen	Steel grade		L	t_1	t_2	B_1	B_2	d_1	d_2
	web	flange	[mm]	[mm]	[mm]	[mm]	[mm]	[mm]	[mm]
RS4-700A	S700MC	S700MC	698.8	4.17	4.11	199	200	280	281
RS4-700B	S700MC	S700MC	699.5	4.10	4.10	200	200	280	281
RS4-H	S700MC	S355MC	698.5	4.11	4.16	198	199	279	279
RS6-355	S355MC	S355MC	799.0	6.20	6.19	219	220	310	310
RS6-700	S700MC	S700MC	798.5	6.10	6.17	220	219	310	309
RS6-H	S700MC	S355MC	798.5	6.10	6.17	220	219	309	309
RS8-700A	S700MC	S700MC	697.8	8.07	7.97	200	199	280	280
RS8-700B	S700MC	S700MC	698.5	7.98	8.00	198	199	280	280
RS8-H	S700MC	S355MC	698.5	7.94	7.94	200	199	281	281

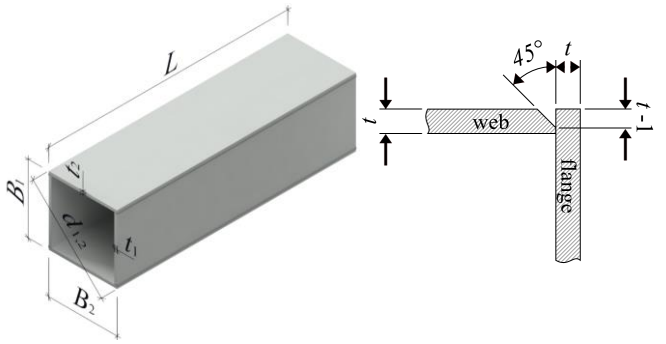

Fig. 1 Sketch of the investigated welded box sections

Table 2 Mechanical properties of base materials according to inspection certificates. [1]

Steel grade	f_y [MPa]	$f_{p0.2}$ [MPa]	f_u [MPa]	A [%]
S355MC – t4	402	-	469	37
S355MC – t6	446	-	570	27
S355MC – t8	400	-	486	30
S700MC – t4	-	746	829	22
S700MC – t6	-	749	833	20
S700MC – t8	-	738	827	22

Table 3 Welding variables of the analysed specimens. [1]

Welding sequence	Specimen	#	-	I [A]	U [V]	V [mm/s]	q [kJ/mm]
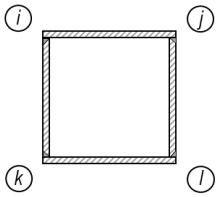	RS4-700A	1	*k*	220	19.5	7.45	0.46
		2	*i*	205	19	7.78	0.40
		3	*j*	192.5	18.5	7.78	0.37
		4	*l*	200	18.5	8.14	0.36
	RS6-H	1	*i*	222.5	23.25	7.77	0.53
		2	*k*	215	22.75	7.55	0.52
		3	*l*	225	22.75	7.69	0.53
		4	*j*	222.5	22.75	7.41	0.55
	RS8-H	1	*k*	215	21.75	12.96	0.29
		2	*i*	205	20.75	11.11	0.31
		3	*j*	205	20.25	11.48	0.29
		4	*l*	205	20.25	10.61	0.31
		5	*k*	205	23.75	7.53	0.52
		6	*i*	220	24.25	7.61	0.56
		7	*j*	220	24.75	8.05	0.54
		8	*l*	232.5	24.25	8.14	0.55

A comprehensive testing program was carried out, incorporating strain gauge measurements, macroscopic inspections, dimensional evaluations, and high-resolution residual stress measurements using the contour method. Among the measurements, the contour method played an important role, which is a destructive residual-stress measurement technique based on Bueckner's superposition principle [2]. It can be regarded as an efficient residual stress measurement technique, since its mean standard deviation (22-34 MPa) in orthotropic steel decks [3] is comparable to the scatter reported for established methods such as neutron and x-ray diffraction (20-40 MPa) [4]. The specimen is cut in two along the centre cross-section using wire electrical discharge machining (WEDM), while being rigidly clamped during cutting. The WEDM releases residual stresses and causes elastic out-of-plane deformation of the new cut surfaces. These deformed surfaces are then measured with a coordinate measuring machine (CMM). The measured deformation fields on the two cut surfaces are averaged, filtered and smoothed using thin-plate smoothing spline. Smoothing is applied according to the methodology recommended by Olson et al. [5], assuming that 68% of the pointwise model errors across the cross-section fall within the mean smoothing-model error. This corresponds to a $\pm 1\sigma$ confidence interval (68%). Smoothed displacement data are mapped onto a linear elastic finite element (FE) model as displacements with opposite sign to compute the full two-dimensional residual stress distribution across the cutting surface. The measurement method allows for accurate quantification of both membrane and through-thickness residual stresses (Fig. 2), from welding and preceding fabrication steps, which serve as crucial input parameters for structural design and numerical modelling.

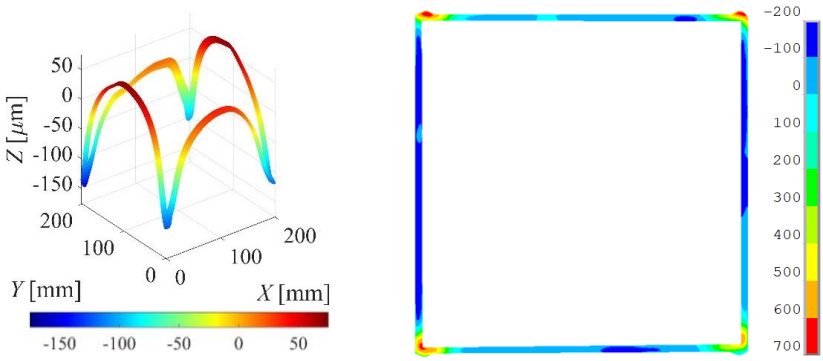

Fig. 2 Example for measured cut surface [μm], and longitudinal residual stress field [MPa]

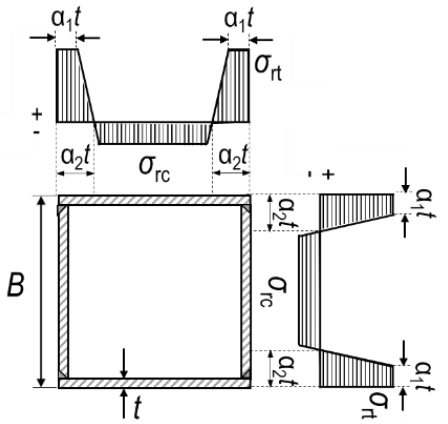

$$\alpha_1 = 1.0$$
$$\alpha_2 = -0.3224 \times qA_{w,nom} + 5.6908$$
$$\varepsilon_{rs} = [400 / \max(f_{y.filler}, f_{y,fl}, f_{y.w})]^{1/2}$$
$$\sigma_{rt} = \varepsilon_{rs} \times \max(f_{y.filler}, f_{y,fl}, f_{y.w}) \times n_{w,pass}^{-2/3}$$
σ_{rc} based on equlibirium

Fig. 3 Previously proposed residual stress model for welded box sections

The results confirmed the theory presented in previous publications [6,7] that the magnitude of residual compressive stress decreases with increasing plate thickness. This is related to the reduction of the weld melt zone and confirms the stress-relieving effect of multiple welding passes. The previous study proposed a novel residual stress model (Fig. 3) for NSS, HSS, and hybrid welded box sections, incorporating parameters such as heat input q, nominal total cross-sectional area of a single-bevel butt weld seam $A_{w,nom}$, number of weld passes n_{wpass}, steel grades of web $f_{y,w}$, flange $f_{y,fl}$ and filler material $f_{y,filler}$. The residual stress model proposed previously in that study is developed exclusively based on the results obtained from the contour method. When compared to existing models, the new formulation demonstrated the highest accuracy in predicting both tensile and compressive residual stress magnitudes, with mean errors of 2.3% and 10.7%, respectively. Its effective application to hybrid box sections represents a notable step forward in the field of design-focused residual stress modelling.

BACKGROUND OF THE NUMERICAL MODEL

The numerical framework presented in this study is developed in ANSYS, a general-purpose finite element software [8] to simulate the thermomechanical effects of welding in welded box sections. A three-dimensional transient uncoupled thermomechanical analysis is applied. Phase transformations are not considered directly, as there is no explicit phase-transformation simulation in the HAZ (heat-affected zone). However, the thermal material model employs an enthalpy-based formulation (replacing density and specific heat), in which the latent heat associated with the $\alpha \rightarrow \gamma$ phase transformation is accounted for in the enthalpy calculation. In addition, phase-transformation strain and creep strain increments are neglected in the simulations. The finite element (FE) model utilizes eight-node solid elements, SOLID70 for the thermal domain and SOLID185 for the mechanical analysis, with mesh refinement in the vicinity of the weld. A double ellipsoidal heat source model is

implemented to represent the metal active gas welding process. Temperature-dependent thermal and mechanical properties are defined based on EN 1993-1-2 [9], with specific adjustments for high-temperature behaviour. The standard does not distinguish between thermal material properties of normal strength steels with different steel grades (material properties could be used without any modification for structural steel grades up to S700 according to EN 1993-1-12 [9]). Material properties are specified up to 1200 °C in the standard, however, the weld pool temperature significantly exceeds this during welding. Therefore, thermal material properties in general are adjusted, while mechanical properties are set as constant values above the zero-strength temperature (T_{zs} = 1200 °C). As an important remark, the material properties specified in the standard have been successfully applied in previous welding simulations [10]. Latent heat is integrated into an enthalpy-based formulation to manage phase changes. In the mechanical model, a rate-independent elastoplastic material model is used, incorporating isotropic hardening. Thermal boundary conditions include convective and radiative heat losses. A comprehensive description of the numerical framework – including the set of temperature-dependent material properties, all relevant input parameters, boundary conditions, and heat source modelling – is provided in detail in [11]. Although the geometry is symmetric, no symmetry is applied in the initial simulations to fully capture the effects of the welding sequence during model validation. To prevent rigid body motion, only minimal mechanical constraints are introduced. In the subsequent probabilistic analyses, double symmetry is applied to (i) reduce computational time and (ii) investigate extreme residual stress scenarios.

VALIDATION OF THE NUMERICAL MODEL

Before conducting the probabilistic welding simulations presented in this study, the developed numerical modelling framework is validated against the experimental data described earlier. During the validation process, all relevant data recorded or measured during manufacturing are incorporated into the simulation model. This included the mechanical properties of both base and filler materials based on inspection certificates; measured geometric parameters such as width, height, length, and plate thickness; weld pool characteristics; and welding variables recorded during the process. In addition, the realistic ambient conditions, such as the measured ambient temperature (T_{amb} = 24.2 °C) and fixtures (only rigid body motion is prevented in the model) during manufacturing, were incorporated into the FE model.

The material properties of the weld region are defined by accounting for the dilution of base and filler materials, as observed in macrographic examinations. The yield and ultimate strengths of the simulated weld elements are determined as a linear combination of the strength properties of the constituent materials. In calculating the mechanical parameters, we assume that - analogously to the weld metal chemical composition reported in [12] - the weld metal mechanical properties can also be estimated as a linear mixture of the characteristics of the filler material and the base material. In the case of hybrid box sections, the weld element properties are determined from a combination of the web, the flange, and the weld materials. To improve the accuracy of the simulation, the effects of plasma cutting

on the flange plates are also included in a simplified form. This effect is considered negligible for the web plates, since part of the heat-affected zone (HAZ) is removed during edge preparation, while the edge is remelted during welding. Before welding, the nodal temperatures at the edges of the flange plates are raised to the liquidus temperature (1525 °C) of the base material, then allowed to cool to ambient temperature prior to the start of welding. The resulting thermal fields are subsequently transferred to the mechanical analysis phase, in the same manner as the welding-induced temperature fields, where the plasma cutting-induced residual stresses are also evaluated.

First, the fusion zones from thermal simulations of box sections with wall thicknesses of 4 mm (RS4-700A from HSS), 6 mm (RS6-H with hybrid configuration), and 8 mm (RS8-H with hybrid configuration) are compared to experimental macrographs of specimens with matching geometries, materials, and welding variables (Fig. 4). This comparison validates the accuracy of the thermal analysis across varying wall thicknesses. The experimental and simulated cross-sectional areas of weld metal (WM) are as follows (without the excess weld metal): 19.4 mm² and 21.7 mm² for $t = 4$ mm, 28.6 mm² and 28.8 mm² for $t = 6$ mm, and 34.0 mm² and 31.0 mm² for $t = 8$ mm, respectively. These results indicate a relatively small average difference of less than 10%. On the other hand, the experimental and simulated effective throat thickness values are 4.0 mm and 4.0 mm (indicating full penetration) for $t = 4$ mm, 5.2 mm and 4.7 mm for $t = 6$ mm, and 6.3 mm and 6.2 mm for $t = 8$ mm, respectively, resulting in an average deviation of approximately 4%. The 8 mm thick specimen features two-pass single-bevel butt welds, while the remaining two specimens are fabricated with single-pass welds.

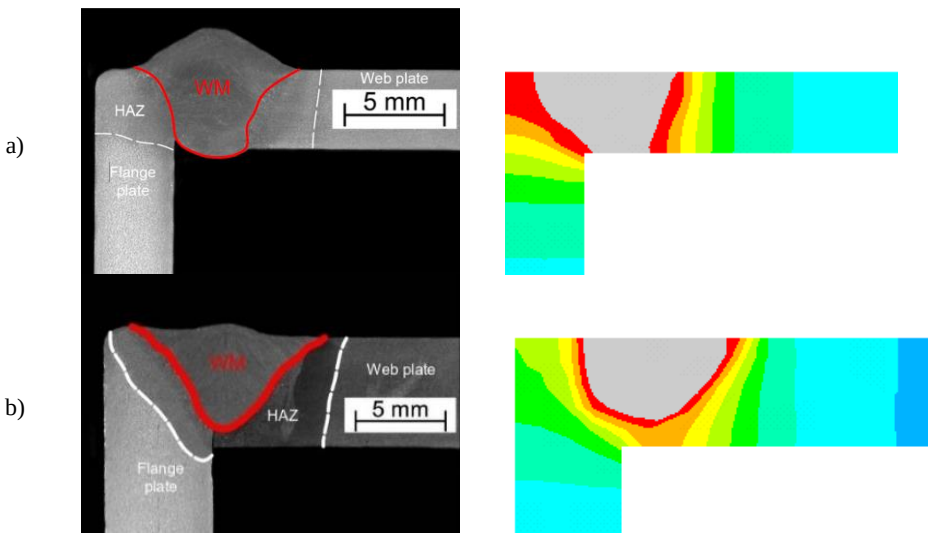

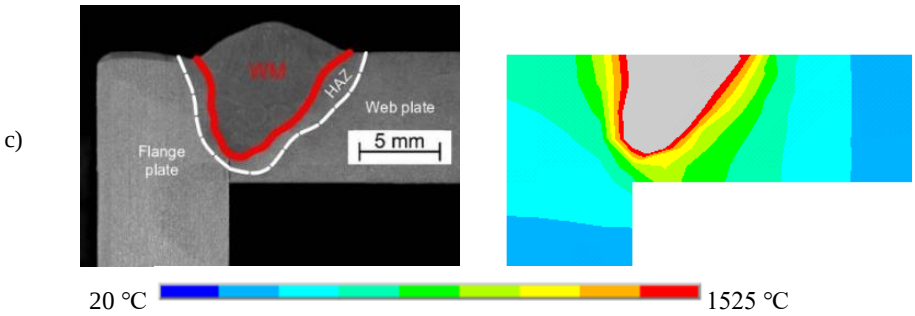

Fig. 4 Macrographs [1] and FE model-based fusion zones of box sections with wall thickness of a) 4 mm (single-pass weld, RS4-700A), b) 6 mm (single-pass weld, RS6-H), and c) 8 mm (two-pass weld, RS8-H)

Additionally, longitudinal residual stresses obtained via contour method measurements are compared with those predicted by the welding simulation. Contour method provides two-dimensional full-map residual stresses; details of the measurement technique and the evaluation are detailed in [1]. In both cases, midsections of the specimens are analysed. The investigated specimen with thickness of 4 mm is a high strength steel box section (RS4-700A). Constituent plates have proof strength of 753 MPa, while the weld material is considered to have a proof strength of 737 MPa in the model according to the dilution-based approach. The other two box sections are hybrid sections (RS6-H and RS8-H combining NSS plates with yielding plateau and HSS plates with proof strength). Yield strength of the flanges is 446 MPa and 400 MPa, while proof strength is 749 MPa and 738 MPa for the webs in the hybrid specimens with wall thickness of 6 mm and 8 mm, respectively. Material model of the weld metal has a proof strength of 696 MPa and 671 MPa for t = 6 mm and t = 8 mm, respectively.

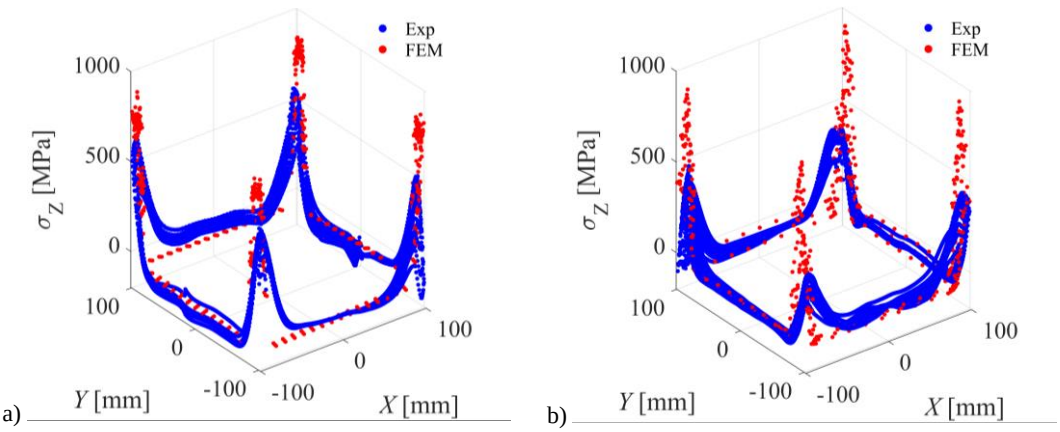

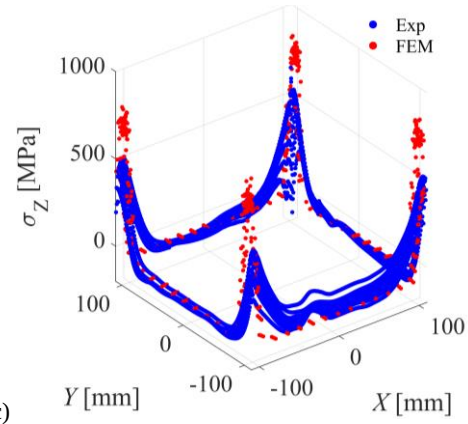

c)

Fig. 5 Measured ('Exp') and numerical model-based ('FEM') longitudinal stresses σ_z of box sections with wall thickness of a) 4 mm (single-pass weld, RS4-700A), b) 6 mm (single-pass weld, RS6-H), and c) 8 mm (two-pass weld, RS8-H)

Fig. 5 summarize the longitudinal residual stress distributions of the characteristic section in the case of the HSS and hybrid box sections. Simulated compressive stresses are between 63 and 100 MPa in the web plate, while they vary between 74 and 115 MPa based on the experiment for t = 4 mm (RS4-700A from HSS). Moreover, a compressive residual stress range of 66-87 MPa and 64-100 MPa is determined based on simulation and measurement, respectively, for t = 6 mm (RS6-H with hybrid configuration). In addition, the hybrid cross-section with t = 8 mm (RS8-H) results in measured compressive residual stresses of 41-115 MPa and simulated magnitudes of 31-95 MPa (quite significant bending in the constituent plates). These results indicate a good agreement between welding simulation and experimental results. Larger discrepancies only occur in the vicinity of the weld beads, where numerical results locally overestimate the measured tensile residual stresses.

PROBABILISTIC WELDING SIMUALTION

The welding simulation model presented is also employed in probabilistic finite element analyses to estimate the distribution of residual stresses in HSS box sections, while refining residual stress model parameters on a stochastic basis. For this purpose, the Probabilistic Design System (PDS) module of ANSYS is used to carry out the probabilistic calculations. The selected probabilistic design variables, along with their corresponding distribution types and parameters, are listed in Table 4, following the guidelines of JCSS [13] and the relevant standard [14] for welding-related parameters. In total, five probabilistic parameters are considered, as summarized in Table 4.

Table 4 Probabilistic variables of welding simulation.

Probabilistic input variable		Distribution function	Distribution parameters
Heat source power	$Q = \eta UI$	Gaussian	$Q_{mean.t4}$ = 2500 W $Q_{mean.t6}$ = 5200 W $Q_{mean.t8.r}$ = 3900 W $Q_{mean.t8.c}$ = 3900 W $\sigma_Q = 0.10 \times Q_{mean}$
Welding speed	v	Gaussian	v_{mean} = 5 mm/s $\sigma_v = 0.10 \times v_{mean}$
Plate thickness	t	Gaussian	t_{mean} = 4 – 6 – 8 mm $\sigma_t = 0.05 \times t_{mean}$
Proof strength	$f_{p0.2}$	Lognormal	$f_{p0.2,mean}$ = 787.2 MPa $\sigma_{fp0.2} = 0.07 \times f_{p0.2,mean}$
Young's modulus	E	Lognormal	E_{mean} = 200 000 MPa $\sigma_E = 0.03 \times E_{mean}$

The heat source power varies depending on the wall thickness of the box sections (indicated as 't4', 't6' and 't8' in the subscript). For the box section with t = 8 mm, which has two weld passes, r refers to the root pass and c to the cover pass. As previously introduced, three distinct geometries are investigated in the probabilistic welding simulation, combining three different plate thicknesses with two plate widths. Specifically, the study included a 200×200 mm box section with nominal wall thickness of 4 mm and 8 mm, as well as a 220×220 mm box section with a nominal plate thickness of 6 mm. Steel grades of the high strength steel constituent plates and the filler material are assumed to be matching. The investigated section is manufactured from S700 steel. Thus, the mean value is calculated from the 5% quantile value by using $f_{p0.2,mean}$ = 700 MPa / 0.8892 = 787.2 MPa. The applied temperature-dependent material models are based on the reduction factors in EN 1993-1-2. However, a temperature-dependent Ramberg-Osgood material model is used for describing the relationship between stresses and strains according to Equation 1 for high strength steels without a yielding plateau. Proof strength is used in the equation instead of yield strength, while n is taken as 14 for high strength steels based on material tests in [15].

$$\varepsilon(\sigma) = \sigma/E + 0.002\,(\sigma/f_{p0.2})^n \tag{1}$$

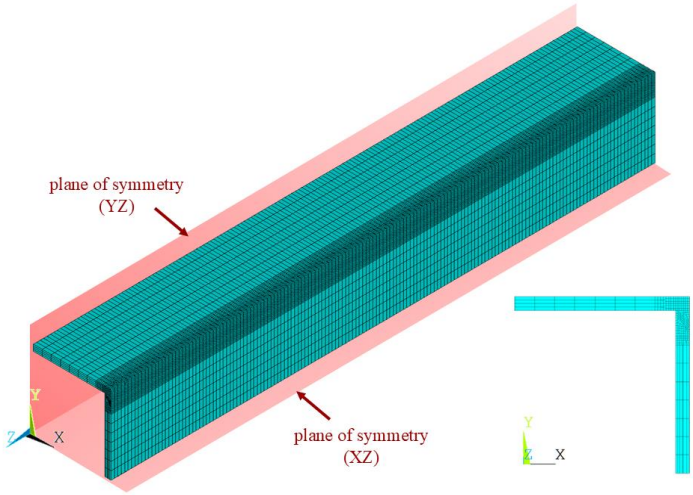

Fig. 6 Quarter model of the box section used in the probabilistic welding simulation

The probabilistic welding simulation utilizes a quarter cross-section model of the box section (Fig. 6) with a width B of either 200 mm or 220 mm, taking advantage of its double symmetry to minimize computational time. Accordingly, the simulation assumes simultaneous welding, neglecting the effect of welding sequence in order to represent the extreme residual stress scenario.

The probabilistic analysis is conducted using Monte Carlo simulation combined with Latin hypercube sampling, a method that ensures statistically independent samples by avoiding clustering and maintaining awareness of previously generated values. On the other hand, extreme ends of distribution functions are also considered in sampling process. A total of N samples is used in the simulation dividing each random input variable into intervals of equal probability ($p = 1/N$), while random sampling is carried out within each interval. Three output variables are analysed, including α_1 and α_2 representing the characteristic widths of the tensile zone and σ_{rt} as the magnitude of membrane tensile residual stresses as indicated in Fig. 3 previously. On the other hand, the compressive residual stress magnitude σ_{rc} is derived from the equilibrium of internal forces and moments in the proposed residual stress model; thus, no regression is carried out in that case. The quantity of simulation loops, i.e., samples, needed for a Monte Carlo simulation to model a quadratic response surface depends on the number of random input variables (n_{RV}, which is 5 in this case). The sample size is defined as 27, in accordance with the advanced analysis guide of the software for the given number of probabilistic design variables. The quadratic response surface is described by Equation 2 as follows:

$$Y = c_0 + \sum_{i=1}^{n_{RV}} c_i X_i + \sum_{i=1}^{n_{RV}} \sum_{j=1}^{n_{RV}} c_{ij} X_i X_j \tag{2}$$

where Y is the approximation function, i.e., a quadratic polynomial in this case, for each output variable, c_0, c_i and c_{ij} are the coefficients of the constant term, the linear terms and the quadratic terms, respectively, while X_i and X_j are the input variables. To evaluate the coefficients for each output variable, a regression analysis is used such that the sum of squared differences between the true simulation results and the values of the approximation function is minimized.

First, all the longitudinal residual stress data in the midsection are plotted (Fig. 8a) for a total of 3×27 simulations indicating three different nominal wall thicknesses. The key numerical results are summarised in Fig. 7 to describe the specific longitudinal residual stress ranges in the three analysed cross-sections:

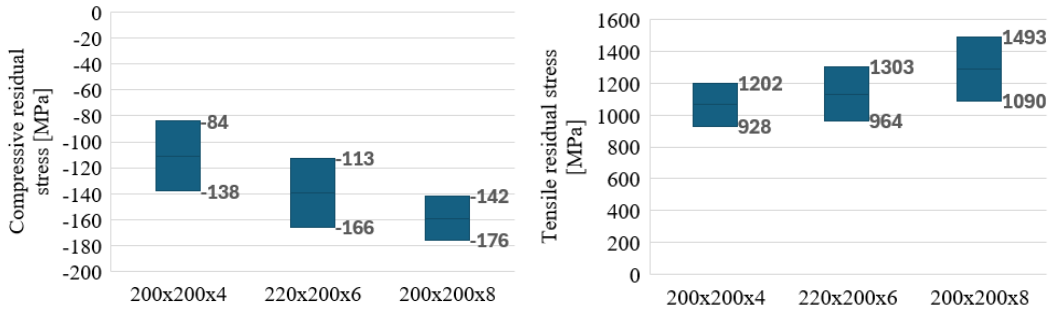

Fig. 7 a) Maximum compressive residual stresses and b) peak tensile residual stresses of analysed box-sections

Secondly, membrane residual stresses are extracted (Fig. 8b) from the full two-dimensional residual stress fields (Fig. 8a). These curves enable the determination of tensile zone widths ($\alpha_1 t$ and $\alpha_2 t$) and the corresponding magnitude of membrane tensile residual stresses σ_{rt}. Then, the probabilistic sensitivities of Spearman rank-order correlation coefficients are determined, assuming a nonlinear monotonic increasing correlation between inputs and outputs (Fig. 9). However, it is acknowledged that the certainty of this assumption regarding a monotonically increasing relationship is not guaranteed. It is highlighted that heat source power Q and wall thickness t have a dominant influence on the tensile zone width (i.e., on α_1 and α_2). Among the considered parameters, the heat source power Q, plate thickness t, and proof strength $f_{p0.2}$ are found to be statistically significant, whereas the remaining parameters are statistically insignificant at a significance level of 2.5%. Based on the limited number of real experiments, α_1 was assumed to be 1.0 indifferently of the manufacturing specialities. Meanwhile, the previously fitted equation for α_2, which was calibrated against experimental test results [1], included the heat input and the nominal cross-sectional area of the single-bevel butt weld (which is proportional to $\sim t^2$), with a minus sign indicating a negative correlation. It needs to be underscored, that a wider range of welding speed v would most probably have resulted in a significant input variable for α_1 and α_2 as heat input is directly calculated based on heat source power and welding speed. Nevertheless, wall thickness t and proof strength $f_{p0.2}$ are statistically significant in the case

of σ_{rt}. Thus, heat input does not significantly affect the maximum membrane tensile residual stresses. Wall thickness indicates negative correlation, which means that increasing the thickness results in decreased membrane stresses in the weld zone. It is in accordance with theory and practice, since welding may lead to tensile stresses even exceeding the yield strength (or proof strength) locally, while stress gradients and through-thickness stresses could be substantial for larger plate thicknesses. In addition, a positive correlation is observed with proof strength, which is expected. Local material hardening may occur due to the highly nonuniform temperature field and high temperature (i.e., large thermal strains).

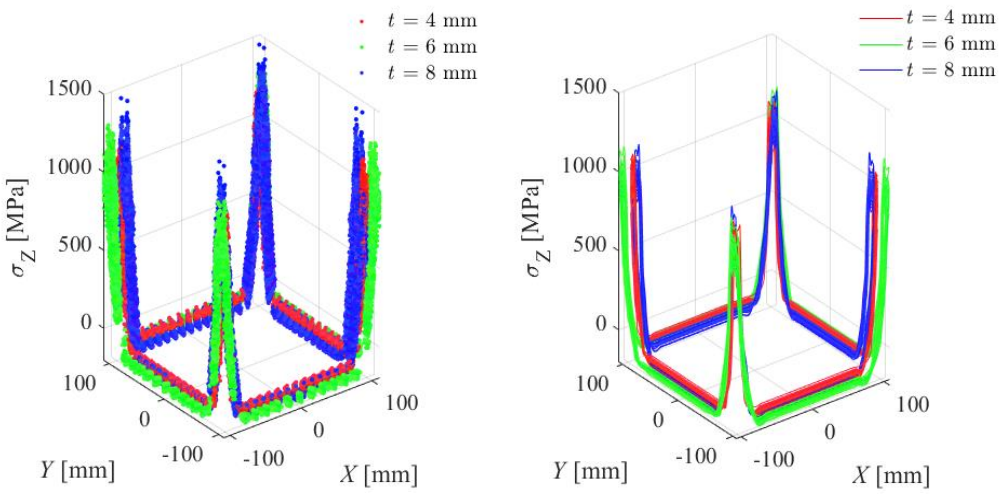

Fig. 8 a) Longitudinal residual stress fields, and b) membrane longitudinal residual stresses from 3×27 probabilistic simulations (t = 4 mm, 6 mm, and 8 mm). Note: double symmetry is used in plotting

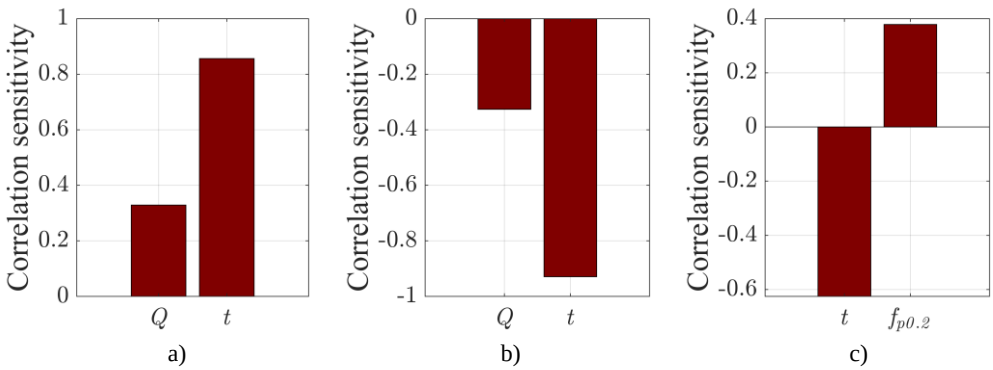

Fig. 9 Spearman rank-order coefficients for a) α_1, b) α_2 and c) σ_{rt}

Finally, the identified coefficients of the significant parameters (Table 5) used in Equation 2, along with the corresponding quadratic response surfaces (Fig. 10), are presented. The output variables include the dimensionless tensile zone width parameters (namely α_1 and α_2) and the membrane tensile residual stress σ_{rt} expressed in [MPa]. The input variables considered in the quadratic polynomial formulations are the welding heat input Q [W], plate thickness t [mm], and proof strength $f_{p0.2}$ [MPa]. By substituting the determined coefficients into Equation 2, the output variables can be predicted within the parameter ranges covered by the probabilistic analysis. For each output variable, two input parameters are identified as significant, resulting in six coefficients per quadratic response surface: one constant, two linear terms, and three quadratic terms (including a cross-term). This modelling approach enables efficient prediction of residual stress characteristics in welded box sections; however, its applicability is currently restricted to the investigated parameter set.

Table 5 Significant coefficients of the response surfaces. Note: N/A denotes insignificant term.

			Output variable		
			α_1	α_2	σ_{rt}
Input variable	c_0	c_0	-8.43552	17.34415	648.9199
	c_i	Q	0.001071	0.001709	N/A
		t	-0.12544	-1.99262	34.88991
		$f_{p0.2}$	N/A	N/A	3.054726
	c_{ij}	$Q \times t$	-0.00013	-8.01E-05	0.030953
		$t \times f_{p0.2}$	N/A	N/A	-0.25115
	c_{ii}	Q^2	9.44E-08	-5.97E-08	N/A
		t^2	0.061392	0.124045	-5.64496
		$f_{p0.2}^2$	N/A	N/A	0.000225

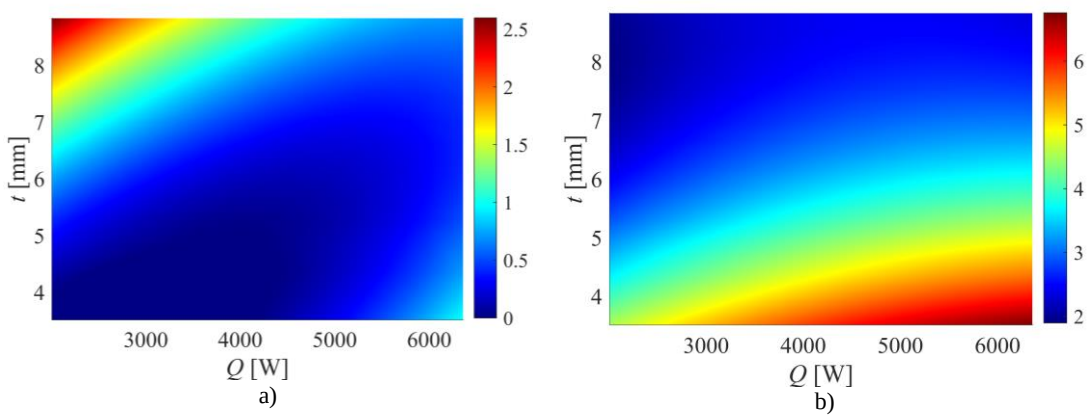

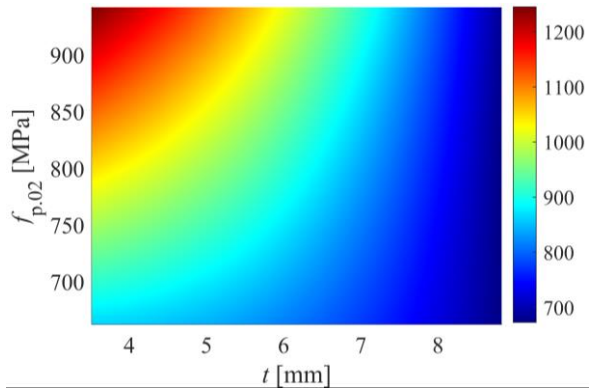

c)

Fig. 10 Response surfaces for a) α_1, b) α_2 and c) σ_{rt} with the statistically significant terms

CONCLUSIONS

The paper presents a comprehensive numerical simulation method for modelling thermal cutting and welding, while a probabilistic residual stress model is proposed considering manufacturing specialities. The paper reveals the following key findings:

- The thermal model is validated by comparing temperature fields with macrographs; average difference of the cross-sectional area of the weld metal is less than 10%, while an average deviation of approximately 4% is achieved in penetration depth.
- The mechanical model is validated by comparing predicted and measured longitudinal residual stresses in both high strength steel and hybrid (consisting of both NSS and HSS plates) box sections. A difference of less than 20 MPa is revealed in the compressive residual stress magnitudes in a comparison with contour method-based results.
- The methodology for probabilistic welding simulation is presented, serving as a basis for subsequently refining the parameters of residual stress models.
- Parameters of a residual stress model, consisting of trapezoidal shapes, previously proposed by the Authors are refined for welded high strength steel (S700) box sections with single-bevel butt welds. Predictions are limited to wall thickness of 4 to 8 mm with single or two weld passes.

Future research will focus on extending the probabilistic framework to incorporate additional stochastic input parameters (such as a wide range of width and yield strength values, also considering hybrid cross-sections), while using equations with thermophysical background for regression instead of the quadratic response surface used in the conventional Monte Carlo simulation.

ACKNOWLEDGEMENTS

This research was funded by Hungarian Academy of Sciences, grant number MTA-BME Lendület LP2021-06/2021 “Theory of new generation steel bridges” program. The research reported in this paper and carried out at the Budapest University of Technology and Economics has been supported by the Ministry for Culture and Innovation from source of the National Research, Development and Innovation Fund, grant number ÚNKP-23-3-I-BME-194 (New National Excellence Program). The project supported by the Doctoral Excellence Fellowship Programme (DCEP) is funded by the National Research Development and Innovation Fund of the Ministry of Culture and Innovation and the Budapest University of Technology and Economics, under a grant agreement with the National Research, Development and Innovation Office. The project supported by the University Research Scholarship Programme (EKÖP) is funded by the National Research Development and Innovation Fund of the Ministry of Culture and Innovation and the Budapest University of Technology and Economics, under a grant agreement with the National Research, Development and Innovation Office.

References

[1] A. HORVÁTH, D. KOLLÁR, B. KÖVESDI: ‘Distortions and residual stresses of NSS, HSS and hybrid box sections with single-bevel butt welds: An experimental study’, *Thin-Walled Structures*, Vol. 208, 112834, doi: 10.1016/j.tws.2024.112834, 2025.

[2] H. BUECKNER: ‘The propagation of cracks and the energy of elastic deformation’, *Transactions of the American Society of Mechanical Engineers*, Vol. 80, pp. 1225-1230, 1958.

[3] D. KOLLÁR, I. VÖLGYI, A. L. JOÓ: ‘Development of residual stress model of orthotropic steel decks using measurements’, *Structures*, Vol. 58, 105601, doi: 10.1016/j.istruc.2023.105601, 2023.

[4] J. D. LORD, A. T. FRY, P. GRANT: ‘A UK residual stress intercomparison exercise – an examination of the XRD and hole drilling techniques’, National Physical Laboratory, *Report CMMT(A) 98*, 2002.

[5] M. D. OLSON, A. T. DEWALD, M. B. PRIME, M. R. HILL: ‘Estimation of uncertainty for contour method residual stress measurements’, *Experimental Mechanics*, Vol. 55, No. 3, pp. 577-585, doi: 10.1007/s11340-014-9971-2, 2015.

[6] L. CHEN, T. WANG, J. PAN, N. MA, R. WANG: ‘Welding Residual Stress Distribution of U-Rib Stiffened Plates of Steel Box Girders and its Influence on Structural Natural Frequencies’, *Frontiers in Materials*, Vol. 9, 876111, doi: 10.3389/fmats.2022.876111, 2022.

[7] C. OLSSON: *Design Handbook for welded steel products*, 6th ed., Techstrat Publishing, Onsala, 2017.

[8] ANSYS INC.: *ANSYS. version 19.5*, Canonsburg, Pennsylvania, USA, 2019.

[9] EUROPEAN COMMITTEE FOR STANDARDIZATION: *EN 1993-1-2:2005 Eurocode 3: Design of steel structures – Part 1-2: General rules – Structural fire design*, Brussels, 2005.

[10] D. KOLLÁR, B. KÖVESDI, J. NÉZŐ: Numerical simulation of welding process – application in buckling analysis, Periodica Polytechnica Civil Engineering, 61 98-109., doi: 10.3311/PPci.9257, 2017.

[11] A. HORVÁTH, D. KOLLÁR: 'Dimensional Analysis and Validity of Uniaxial Residual Stress Distribution for Welded Box Sections', *Journal of Manufacturing and Materials Processing (JMMP)*, Vol. 9, No. 1, 5, doi: 10.3390/jmmp9010005, 2025.
[12] Y. L. SUN, C. J. HAMELIN, T. F. FLINT, A. N. VASILEIOU, J. A. FRANCIS, M. C. SMITH: 'Prediction of Dilution and Its Impact on the Metallurgical and Mechanical Behavior of a Multipass Steel Weldment', *Journal of Pressure Vessel Technology* (JPVT), Vol. 141, No. 6, 061405, doi: 10.1115/1.4044337, 2019.
[13] JOINT COMMITTEE OF STRUCTURAL SAFETY (JCSS): *Probabilistic Model Code*, https://www.jcss-lc.org/jcss-probabilistic-model-code/, 2002.
[14] STANDARDS AUSTRALIA / STANDARDS NEW ZEALAND: *AS/NZS 3992:2015 Australian/New Zealand Standard: Pressure equipment – Welding and brazing qualification*, Sydney, 2015.
[15] B. SOMODI: *Flexural buckling resistance of high strength steel welded and cold-formed square closed section columns*, PhD thesis, Budapest University of Technology and Economics, 2018.

APPENDIX

NOMENCLATURE

Symbol	Description	Unit
α_1	relative width parameter of residual stress model	[-]
α_2	relative width parameter of residual stress model	[-]
A	ultimate strain at fracture	[-]
$A_{w,nom}$	nominal total cross-sectional area	[mm²]
B_1	full width of box section	[mm]
B_2	full height of box section	[mm]
c_0	coefficient of the constant term in the quadratic response surface equation	depending on output variable
c_i	coefficient of the linear term in the quadratic response surface equation	depending on output variable
c_{ij}	coefficient of the quadratic term in the quadratic response surface equation	depending on output variable
d_1, d_2	diagonal dimensions of a cross section	[mm]
E	Young's modulus	[MPa]
E_{mean}	mean value of Young's modulus	[MPa]
ε_{rs}	residual stress model factor depending on yield strength	[-]
η	thermal efficiency	[-]
$f_{p0.2}$	proof strength	[MPa]
$f_{p0.2,mean}$	mean value of proof strength	[MPa]
$f_{y,fl}$	yield strength of flange	[MPa]
$f_{y,filler}$	yield strength of filler material	[MPa]

$f_{y,w}$	yield strength of web	[MPa]
f_u	ultimate strength	[MPa]
I	welding current	[A]
L	length of box section	[mm]
N	number of samples in Monte Carlo simulation	[-]
n_{RV}	number of random input variables	[-]
n_{wpass}	number of weld passes	[-]
q	net heat input	[kJ/mm]
Q	heat source power	[W]
$Q_{mean.t4}$	mean value of heat source power for the 4 mm-thick specimens	[W]
$Q_{mean.t6}$	mean value of heat source power for the 6 mm-thick specimens	[W]
$Q_{mean.t8.c}$	mean heat source power for the 8 mm-thick specimens (cover pass)	[W]
$Q_{mean.t8.r}$	mean heat source power for the 8 mm-thick specimens (root pass)	[W]
σ_E	standard deviation of Young's modulus	[MPa]
$\sigma_{fp0.2}$	standard deviation of proof strength	[MPa]
σ_Q	standard deviation of heat source power	[W]
σ_{rc}	magnitude of compressive residual stress	[MPa]
σ_{rt}	magnitude of tensile residual stress	[MPa]
σ_Z	longitudinal residual stress	[MPa]
t	plate thickness	[mm]
t_1	plate thickness of web	[mm]
t_2	plate thickness of flange	[mm]
T_{amb}	ambient temperature	[°C]
t_{mean}	mean value of plate thickness	[mm]
T_{zs}	zero-strength temperature	[°C]
U	voltage	[V]
v	travel speed	[mm/s]
v_{mean}	average value of welding speed	[mm/s]
X_i, X_j	input variables in the quadratic response surface equation	depending on output variable
Y	approximation function for quadratic response surface	depending on output variable